Energy Migration and Excimer Formation in Quasi-Two-Dimensional Polymer Films As Revealed by the Time-Resolved Fluorescence Depolarization Measurement

Nobuhiro Sato, Shinzaburo Ito,* Kazutoshi Sugiura, and Masahide Yamamoto

Department of Polymer Chemistry, Graduate School of Engineering, Kyoto University, Kyoto 606-8501, Japan

Received: October 14, 1998; In Final Form: February 12, 1999

Excitation energy migration and subsequent energy transfer to excimer-forming sites occurring in a quasi-two-dimensional plane of poly(isobutyl methacrylate) Langmuir−Blodgett films were investigated through the time-resolved analyses of anthracene fluorescence. Fluorescence anisotropy decays showed that the energy migration occurred more efficiently as the anthracene fraction increased. A further increase of the anthracene gave rise to the excimer-forming sites acting as energy traps, and finally the anthracene fluorescence was markedly quenched from the energy transfer to the traps. The migration process was quantitatively analyzed by a computer simulation based on the Monte Carlo method, which allowed estimation of the number of hopping and the mean-square displacement of excitons. The initial growth of the mean-square displacement with time became gradually gentle, while the number of hopping linearly increased with time. This result shows that the excitons are not diffusive and tend to stay within a small cluster of chromophores, especially for small chromophore density at short times.

Introduction

Electronic excitation energy transfer through dipole−dipole interaction has been widely studied as a powerful tool for evaluating nanometer-scale distance because the rate of the transfer markedly depends on the separation distance between an energy donor and an acceptor. Moreover, the fluorescence decay profiles reflect the spatial distribution of the donors and the acceptors so that they provide structural information on the system where the chromophores are embedded. Recent interest in artificially organized molecular assemblies gives more significance to energy-transfer studies on geometrically restricted structures, such as Langmuir−Blodgett (LB) films,[1−7] micelles,[8,9] and the phase-separated structure of block copolymers.[10−12]

On the other hand, the characterization of the transfer process in such specific structures is an interesting issue from the standpoint of photophysics. LB films have been extensively utilized[13−18] to control the chromophore−chromophore distance by changing the layer separation. They also have a feature that the space dimensionality of the system can be varied by changing the number of layers of the built-up film.[19] As a limiting case, a two-dimensional field is obtainable by depositing only a single monolayer. Thus LB films give a unique feature for the energy-transfer studies. Polymer LB films, in particular, have advantages from both applicational and scientific points of view in (1) mechanical and thermal stability, (2) thinness of each layer, and (3) uniform and random dispersion of functional groups. Therefore, numerous studies have been reported on the energy transfer in polymer LB films.[17−20]

The energy transfer is classified into two cases: one is "energy transfer" in a narrow sense, occurring between different kinds of chromophores, and the other is "energy migration" between the same kind. In the former case, the time course of the fluorescence intensity well-characterizes the transfer process; in the latter case, the fluorescence decay does not vary with the migration rate. In practice, however, some energy traps, such as excimers or impurities, often exist, and then the fluorescence quenching can be observed as a result of the migration and the subsequent transfer to the traps. To develop efficient energy transport systems, it is essential to reduce the trap density, keeping the high chromophore density.

Fayer and co-workers[21−23] developed a theory describing the survival probability of an excitation being on the initially excited chromophore even for a case that energy traps exist in the system; this survival probability is directly related to the fluorescence anisotropy. They excellently demonstrated[24] the coincidence between their theory and the experimental results; however, mathematical complexity makes it difficult to be applied to a variety of systems. As will be described below, we studied a double layer of LB films, which was a *quasi*-two-dimensional system, and therefore, it was hard to apply their theory directly to our system. Later, Fayer et al. presented more handy expressions based on the two-particle model, which can be applied to various geometries.[25] They also deal with double layer systems in the paper, but the well-defined expressions are given only when the layer separation is sufficiently large or small relative to the Förster radius. Since the layer separation of our system (∼1 nm) was comparable to the Förster radius (∼2 nm), we could not utilize their treatment. Moreover, while the decay of fluorescence anisotropy is well-described, behavior of migrating excitons cannot be understood from this calculation.

Another effective approach for revealing the characteristics of the excitation energy migration is a computer simulation. By using appropriate models, one can analyze photophysical processes in a variety of systems that are hard to deal with theoretically and also can visualize the motion of the hopping exciton. For example, Ohmori et al.[6] investigated the energy transfer in polymer LB films by using a Monte Carlo simulation based on the Förster kinetics and clarified the relaxation of the layer structure, assuming a Gaussian distribution of chromophores.

* To whom correspondence should be addressed. E-mail: sito@polym.kyoto-u.ac.jp.

10.1021/jp9840735 CCC: $18.00
Published on Web 04/16/1999

TABLE 1: Anthracene Fraction (f) and Weight-Average Molecular Weight (M_w) of Sample Polymers

sample	f/%	$10^{-3} M_w$
A-0.5	0.53	95.6
A-1	1.2	136
A-3	2.7	89.9
A-4	3.7	73.0
A-6	6.0	59.4
A-12	12	52.1
A-23	23	53.5
A-33	33	43.1

In this study, we prepared a quasi-two-dimensional plane by the LB method using anthracene-labeled poly(isobutyl methacrylate) and investigated the fluorescence behavior to reveal the photophysical processes in two dimensions. We also applied a computer simulation based on the Monte Carlo method to the results of the fluorescence depolarization measurement in order to reveal the feature of energy migration in two dimensions.

Experimental Part

Materials. The polymer used was poly(isobutyl methacrylate) (PiBMA), which forms a stable monolayer at the air/water interface and has good transferability onto solid substrates.[26] As a fluorescent probe, various fractions of anthracene moieties were introduced into the side chain. Anthracene has the transition moment along its shorter axis and shows large intrinsic anisotropy. The anthracene-labeled monomer, 9-(10-methylanthryl)methyl methacrylate, was obtained as follows. Commercial 10-methylanthracene-9-carboxyaldehyde (Aldrich) was reduced with $NaBH_4$ in an ethanol solution, and then the product, 9-(10-methylanthracene)methanol, was reacted with methacryloyl chloride in a THF solution. The anthracene-labeled polymer was synthesized by radical copolymerization of isobutyl methacrylate and 9-(10-methylanthryl)methyl methacrylate in a benzene solution with AIBN as an initiator. The polymer obtained was purified through reprecipitation from benzene into methanol three times. Table 1 shows the characteristics of the polymers used. The molecular weights were determined by gel permeation chromatography (GPC) with reference to polystyrene standards. The fractions of anthracene units were determined from the UV absorbance with reference to the molar extinction coefficient of a reference compound, 9-(10-methylanthracene)methanol, which was found to be 9200 cm^{-1} M^{-1} at 377 nm in a dichloromethane solution. Poly(vinyl pentanal acetal) (PVPe), employed for the pre- and overcoating layers, was synthesized by the acetalization of poly(vinyl alcohol) with 1-pentanal. The detailed synthetic procedure was reported elsewhere.[1]

Film Preparation. Quasi-two-dimensional planes were prepared in LB films, the structure of which is depicted in Figure 1. Monolayers were prepared on pure water that was treated with a water purification system (Barnstead NANO Pure II). A benzene solution (ca. 0.1 g L^{-1}) of the polymer was dropped onto the water surface in a Teflon-coated aluminum trough. Twenty minutes after the solution was spread, the monolayer was compressed up to a surface pressure of 10 mN m^{-1} and deposited by the vertical dipping method onto a hydrophobic quartz substrate treated with trimethylchlorosilane in advance. Four layers of PVPe were deposited for pre- and overcoating, respectively, to reduce the influence of the substrate and the quenching by oxygen in the air. The adjacent two layers of PiBMA were deposited as a Y-type film.[27] The film preparation and the measurement of surface pressure−area isotherms were carried out at 20.0 °C.

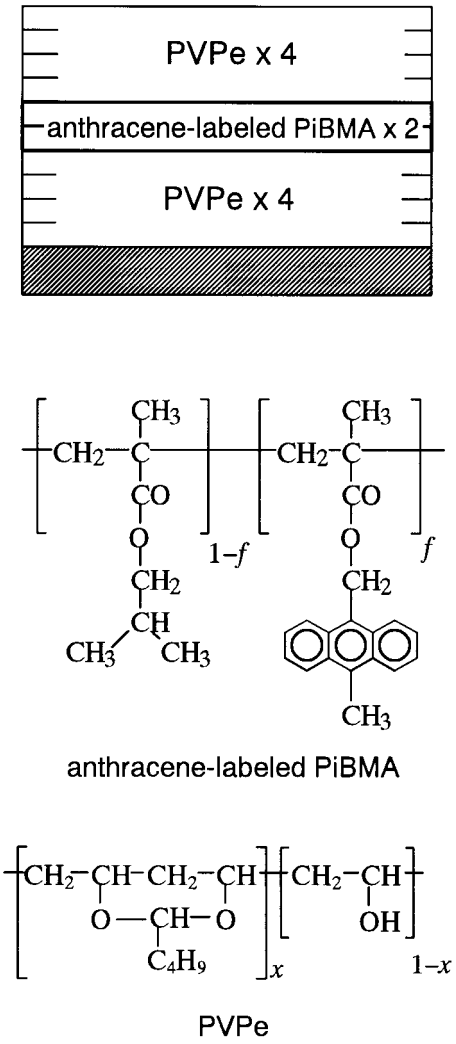

Figure 1. Layer structure of sample LB film.

Fluorescence Measurement. Steady-state fluorescence spectra were measured with a fluorescence spectrometer (Hitachi model 850). Time-resolved measurements were carried out with a time-correlated single photon counting system. A Ti:sapphire laser (Spectra Physics model 3950) pumped by an Ar ion laser (Spectra Physics model 2060) was used as a light source. The beam after passing through a frequency doubler had a wavelength of 398 nm at which anthracene has a sufficient absorbance. The measurement system was setup as follows. An s-polarized excitation beam was introduced into a sample film from the opposite side of a detector with an incidence angle of approximately 45°, and the fluorescence was observed along the plane normal of the sample film. The parallel and perpendicular components were alternately obtained by rotating an analyzer by 90°. Optical filters (SC-42 and B-370) were placed in front of the detector to select monomer emission of anthracene around 430 nm. A diffuser to remove a polarization effect was also placed there. A microchannel-plate photomultiplier (Hamamatsu R3809U) was used as the detector. The full width at half-maximum (fwhm) of the response function was 60 ps.

For the time-resolved fluorescence spectroscopy, both excitation and emission lights were made depolarized with diffusers. An optical filter (SC-41) and a monochromator were installed in front of an end-on photomultiplier (Hamamatsu R3234). The response function had a fwhm of 600 ps.

The Förster radius R_0 for anthracene−anthracene was determined from fluorescence and absorption spectra of a model

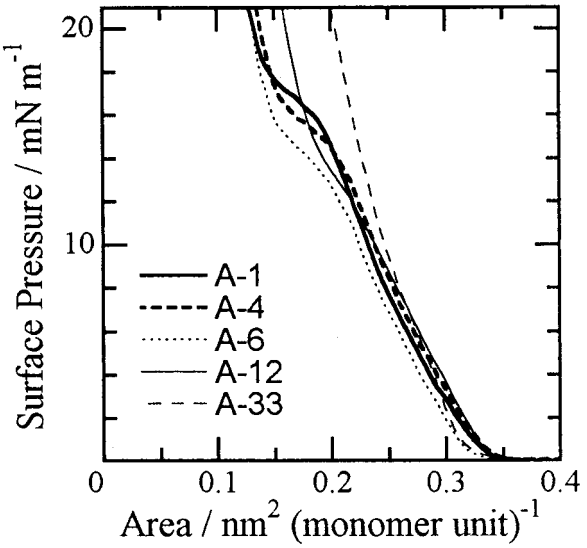

Figure 2. Surface pressure−area isotherms for the monolayers of the polymers studied. The increase in anthracene fraction gave rise to the alteration of the profiles, especially at the large fractions..

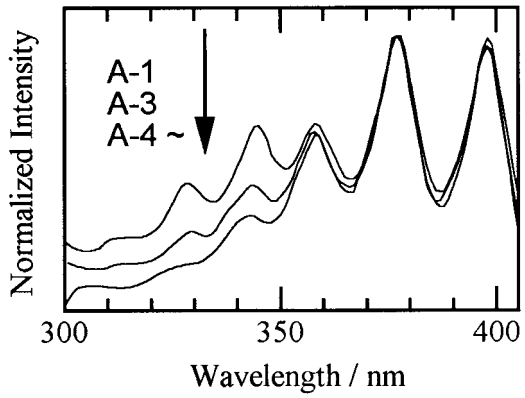

Figure 3. Excitation spectra monitored at 430 nm. These curves are normalized with the intensity at 377 nm. Since the spectra of samples from A-4 to A-33 are nearly identical, they are not shown here for clarity. The emission at wavelengths below 350 nm is ascribed to that from PVPe used for the pre- and overcoating.

compound, 9-(10-methylanthryl)methyl trimethyl acetate in cyclohexane: $R_0 = 2.5$ nm.

Results

Monolayer Property. Surface pressure−area isotherms are shown in Figure 2. At small fractions, the isotherms were similar to that of the unlabeled polymer reported previously.[26] As the fraction increased, however, the surface pressure of the plateau region (ca. 16 mN m^{-1}) decreased. Furthermore, above 10% in fraction, the plateau region disappeared and the slope became steeper. This indicates that the monolayer becomes less compressible as the anthracene fraction increases. The change of the monolayer property affected the transferability of the monolayers onto the solid substrate. While the transfer ratios were close to unity for A-0.5 through A-12, those for A-23 and A-33 were quite smaller than unity and indicate incomplete deposition of these monolayers.

Fluorescence Spectra. Figure 3 shows normalized excitation spectra monitored at 430 nm. The samples with fractions above 4% showed identical spectra that resemble the absorption spectrum of anthracene in solutions or in thick films. This is indicative of no special interaction among the anthracene moieties at the ground state, such as dimer formation. The samples with fractions below 3% showed rather high intensity below 350 nm, owing to the emission of PVPe, which will be mentioned later.

Figure 4a shows normalized emission spectra excited at 377 nm. As the fraction increased, the peak at 400−410 nm became weaker and a broad band around 470 nm became stronger. The emission at shorter wavelengths whose relative intensity increased with decreasing anthracene fraction was attributed to that of PVPe used for the pre- and overcoating layers. Although we employed PVPe as a nonfluorescent polymer, it showed a weak and broad emission over 400−500 nm whose intensity was comparable to that of the anthracene fluorescence at small fractions. The higher intensity at ca. 330 nm in the excitation spectra mentioned before was also ascribed to the PVPe emission.

Emission intensity from the sample films increased with increasing anthracene fraction but then decreased at higher fractions. Figure 4b represents the emission intensity of the peaks at ca. 430 nm as a function of plane density of the anthracene unit, which was measured under the same spectroscopic condition. Although the intensity increased almost in proportion to anthracene density at low densities, yet fluorescene was greatly quenched at densities higher than 0.25 nm^{-2}, the value of which corresponds to the A-6 sample. This behavior will be discussed together with the results of the fluorescence decay measurement.

To investigate the broad band around 450 nm, we examined time-resolved spectra. As shown in the normalized spectra of Figure 5, the relative intensity at 470 nm increased with time for the large fraction samples; therefore, this band can be assigned to the emission of anthracene excimers. A broad band of A-1 at short times is due to the PVPe emission.

Fluorescence Decay. The time course of the total emission intensity, $I(t)$, can be obtained from the parallel and perpendicular components, denoted by $I_{||}(t)$ and $I_{\perp}(t)$, respectively, according to the equation below.[28]

$$I(t) = I_{||}(t) + 2I_{\perp}(t) \tag{1}$$

Figure 6 shows fluorescence decay curves in a logarithmic scale; the excitation wavelength was 396 nm. The decay curves from A-0.5 to A-3 were well-fitted with two-component exponential functions. Judging from the time-resolved fluorescence spectra, the fast decay component with a time constant of ca. 1.5 ns is due to the PVPe emission. Consequently, the time constant of the slow component (12.5 ns) corresponds to the intrinsic lifetime of the anthracene in the LB films, being close to the lifetime of the anthracene moiety in degassed solutions. As the anthracene fraction increased, the fraction of the fast component from PVPe decreased and the decay curves approached a straight line. However, when the fraction was larger than 6%, the curve deviated again from a straight line and did not follow even two-component exponential functions. This deviation indicates the presence of the excitation energy transfer to energy traps. As the anthracene fraction became larger, the quenching occurred more markedly.

Fluorescence Depolarization. The result of the fluorescence depolarization measurement is shown in Figure 7 where fluorescence anisotropy ratio, $r(t)$, is defined by the following equation.

$$r(t) = [I_{||}(t) - I_{\perp}(t)]/[I_{||}(t) + 2I_{\perp}(t)] \tag{2}$$

Since the small fraction samples showed an anomalous rise from PVPe emission in the short time region, we omitted it in the

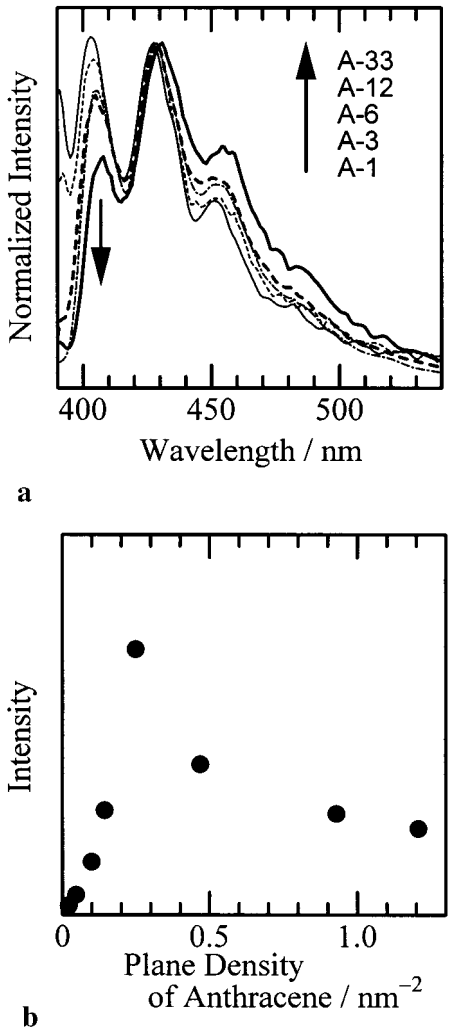

Figure 4. (a) Fluorescence spectra normalized at 430 nm. Emission of the anthracene excimer appears around 470 nm at large fractions. The emission around 400 nm was caused by the PVPe emission. (b) Emission intensity as a function of plane density of the anthracene unit.

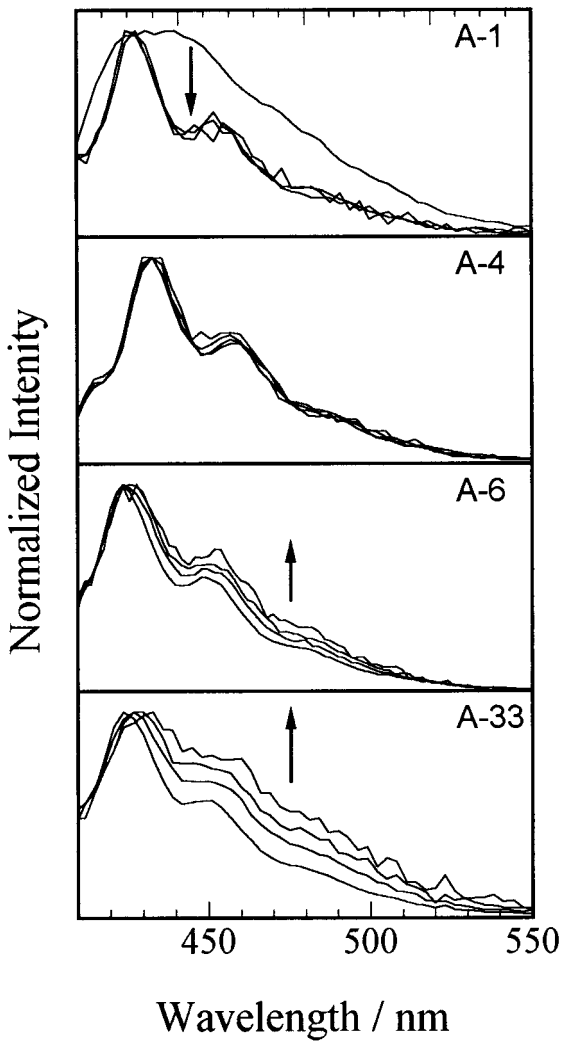

Figure 5. Time-resolved fluorescence spectra. The observed time ranges are 0−1, 10−11, 20−21, and 30−31 ns. The arrows in the figure represent this time order. Especially for A-33, the excimer band becomes prominent as time passes.

following discussion. The anisotropy ratio hardly decayed for A-0.5 and A-1 but decayed faster as the fraction increased. Since the anthracene moieties embedded in the LB films are hardly allowed to rotate, the anisotropy decay is caused only by the energy migration. Consequently, the anisotropy decays indicate that the migration occurred more efficiently with increasing anthracene fraction. For A-23 and A-33, however, the decays became slower despite the large fractions. There may be two reasons for this: (1) a contribution of the long-lived anthracene excimer and (2) incomplete deposition of the monolayers from the air/water interface.

Discussion

Qualitative Schema for the Migration and the Quenching. The monomer fluorescence of the anthracene moieties was appreciably quenched at fractions above 6%. Because the emission of the anthracene excimer became noticeable above 6%, this quenching was attributable to the excimer-forming sites (EFS). Considering the anisotropy decay results, the considerable quenching of the anthracene fluorescence was due not only to an increase of EFS but also to a more vigorous energy migration between the anthracene moieties as the fraction became larger. The apparent transfer distance of the excitation energy became longer because of the migration so that the excited state could be transferred to more EFS. As a summary of the above consideration, we can offer the following qualitative schema. At fractions below 1%, the excited state of the anthracene relaxed without interacting with one another. For 3−6%, energy migration between the anthracene moieties appreciably occurred; however, the monomer fluorescence was hardly quenched because the migration distance was short, and there were only a few EFS. Above 6%, the monomer fluorescence was markedly quenched by the energy transfer to EFS via the efficient energy migration among the anthracene moieties.

Analysis of the Anisotropy Decay. The anisotropy decay curve has a direct relationship with the migration process of the excitation energy. It is consequently possible to explicate the mode of the migration in the two-dimensional system by analyzing the obtained anisotropy decays. The current system is not exactly two-dimensional because the anthracene moieties are distributed in two layers; accordingly, we attempted to simulate the anisotropy decays on the basis of the Monte Carlo method, employing an exciton-hopping model in the double-layer system. Since energy trapping by EFS complicates interpretation of the anisotropy decay data, we focused on the samples from A-0.5 to A-6 in which the quenching by the traps was negligible.

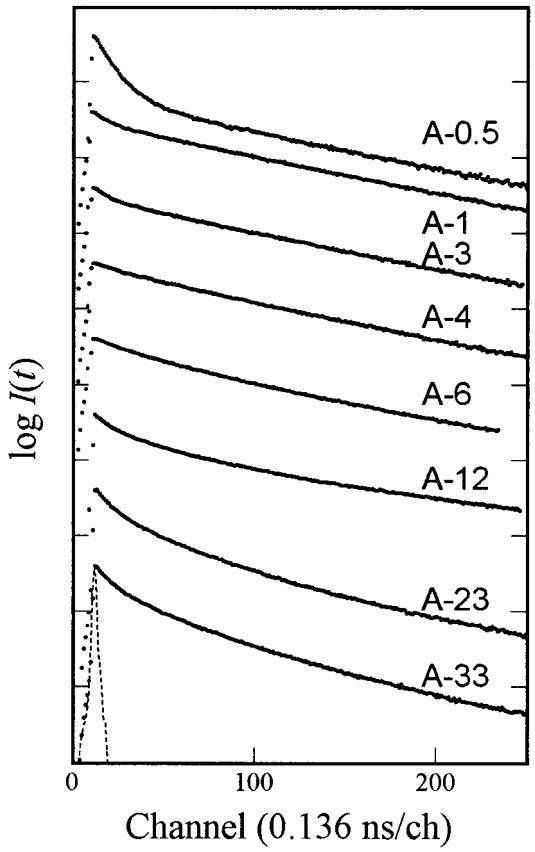

Figure 6. Fluorescence decay curves observed for the excitation at 396 nm. The fast decay observed at short times for A-0.5 is due to the PVPe emission. At small fractions, the curves are fitted with one-component exponential functions, if the short component is neglected. The longer time constant corresponds to the unquenched lifetime of the anthracene in the film. For large anthracene fractions, the curves deviate from a straight line, indicating that the energy transfer to energy traps occurred.

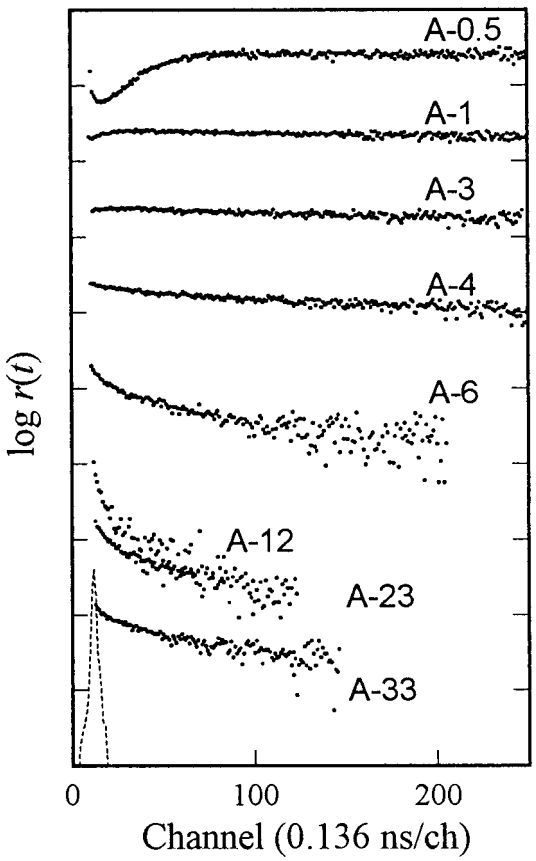

Figure 7. Time course of the measured anisotropy ratio. A-0.5 exhibits an anomalous rise at short times because of the PVPe emission. For the samples with fractions larger than 6%, the efficient energy migration occurred.

Detailed Procedure of the Simulation. Figure 8 schematically illustrates the arrangement of the simulation space. In the beginning, two square regions with a side length of L are placed parallel to each other with a separation of d, and one of the squares is set as the xy-plane. Then N chromophores are distributed as follows. One chromophore with an orientation vector aligning with the y-axis is located at the origin of the xy-plane, and the other $(N - 1)$ chromophores are randomly distributed in the two planes with their transition moment vectors taking random and isotropic orientations. The chromophore at the origin is excited initially. The distributed chromophores are distant enough from one another not to come closer than the excluding area of the chromophore, $\sim$0.28 nm^2. In this condition, ρ, the number density of the chromophores in a single plane, is given as $N/(2L^2)$.

Next, a singlet exciton hops around the chromophores in the following manner, until it is deactivated. First, the migration rate from the currently excited chromophore to every other one is calculated. The orientation factor κ_j^2 of chromophore j with respect to chromophore i is calculated with the following equation.[25]

$$\kappa_j^2 = [\boldsymbol{M}_i \cdot \boldsymbol{M}_j - 3(\boldsymbol{M}_i \cdot \boldsymbol{r}_j)(\boldsymbol{M}_j \cdot \boldsymbol{r}_j)/|\boldsymbol{r}_j|^2]^2 \quad (3)$$

where $\boldsymbol{M}_i$ and $\boldsymbol{M}_j$ are the orientation vectors of a unit length and $\boldsymbol{r}_j$ is a position vector of chromophore j with respect to chromophore i. Then, the migration rate k_j is given below.

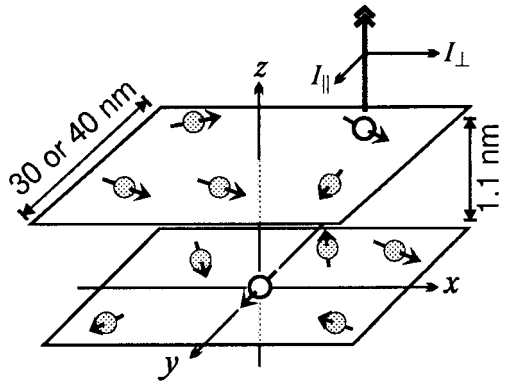

Figure 8. Schematic illustration of the arrangement of the simulation space and the distribution of the chromophores. The x- and y-components of the orientation vector correspond to the $I_\parallel$ and $I_\perp$, respectively.

$$k_j = (3/2)\kappa_j^2 R_0^6 |\boldsymbol{r}_j|^{-6} \tau_0^{-1} \quad (4)$$

where R_0 is the Förster radius for anthracene−anthracene and τ_0 is the intrinsic lifetime of the anthracene. Second, the probability of the migration to chromophore j or that of the deactivation at chromophore i is determined. The former probability, p_j, is given as

$$p_j = k_j/(\sum k_j + \tau_0^{-1}) \quad (5)$$

while the latter, p_d, is given as

$$p_d = \tau_0^{-1}/(\sum k_j + \tau_0^{-1}) \quad (6)$$

The duration time until a next event (migration or deactivation) is determined with a random number following an exponential distribution with a parameter of $(\sum k_j + \tau_0^{-1})$. As long as the exciton is alive, the probability calculation and the exciton migration are repeated.

When the deactivation occurs, that is, the fluorescence is observed, the number of photon counts, $c(t_i)$, is increased by 1 at the channel t_i corresponding to the elapsed time t. Thus, the profile of $c(t_i)$ represents the fluorescence decay. The number of exciton hopping, $h(t_i)$, and the square displacement from the origin, $l^2(t_i)$, are also recorded at t_i. The simulated anisotropy, $r^\circ_{sim}(t_i)$, is calculated with eq 2 where $I_\perp(t)$ and $I_\parallel(t)$ correspond to the squares of the x- and y-components of the orientation vector, respectively.

The above procedure (distribution, hopping, and deactivation) is repeated 10^4-10^5 times, and finally, the averaged curves of $c(t_i)$ and $r^\circ_{sim}(t_i)$ are obtained. The values of $h(t_i)$ and $l^2(t_i)$ are also averaged and then normalized with the value of $c(t_i)$ because the magnitude of $h(t_i)$ and $l^2(t_i)$ depends on $c(t_i)$.

The initial anisotropy ratio $r^\circ_{sim}(0)$ is unity because the initially excited chromophore is always set along the y-axis, but actual initial anisotropy ratio is less than unity because the excitation probability varies with the orientation of excited chromophores. For example, the isotropically random orientation yields 2/5 as the ideal initial anisotropy ratio for linearly polarized excitation. In this simulation, the excitation probability is considered as a constant multiplier to $r^\circ_{sim}(t_i)$. Thus, simulated anisotropy decay curves are given as

$$r_{sim}(t_i) = r_0 \cdot r^\circ_{sim}(t_i) \tag{7}$$

where r_0 is the initial anisotropy ratio. In principle, r_0 can be determined theoretically if the orientation of chromophores are known; in practice, however, the experimental initial anisotropy ratio is often different from the theoretical one. Therefore, r_0 was determined so that the experimental decay curves for different ρ values might be best fitted with the same r_0 value.

Prior to executing the simulation, we checked its validity in the following two ways. (1) We applied the simulation for a three-dimensional system after modifying the distribution of the chromophores and compared with an experimental anisotropy decay measured for a spin-coated thick film (ca. 0.5 μm thick) of A-0.5. By using spectroscopically obtained R_0 (Förster radius), the simulation curve coincided with the experimental one. This coincidence not only shows the validness of the simulation but also indicates that R_0 obtained for the model compound in cyclohexane solution is acceptable for the LB films as mentioned in Experimental Part. (2) The model was modified for exactly two dimensions, and the simulated curves were compared with the theoretical expression developed by Baumann and Fayer.[25] When their theory is applied to our case in which chromophores were distributed in two dimensions with static and isotropic orientation, the $r^\circ_{sim}(t)$ under the polarized excitation parallel to the plane is given by

$$r^\circ_{sim}(t) = \exp[-A(t/\tau_0)^{1/3}] \tag{8}$$

with

$$A = \rho\pi R_0^{\,2} 2^{-2/3}(3/2)^{1/3}\langle|\kappa|^{2/3}\rangle\Gamma(2/3) \tag{9}$$

where $\Gamma(2/3)$ is a gamma function and $\langle|\kappa|^{2/3}\rangle$ equals 0.7641. The simulated curves followed well this expression, also indicating the validness of our simulation model.

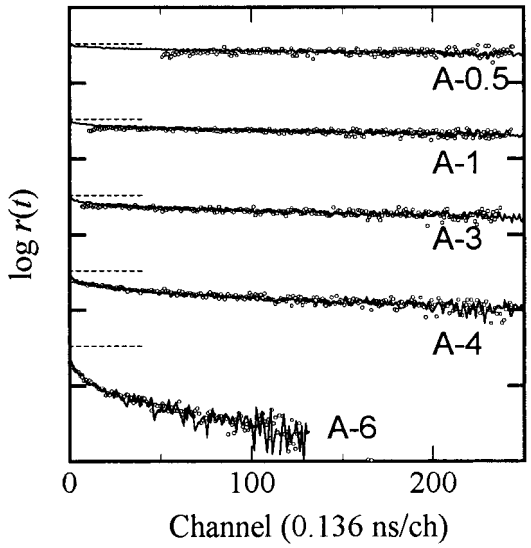

Figure 9. Comparison of the simulated curves with the experimental decays. The broken lines in the figure indicate the initial anisotropy r_0. Fine results are obtained with ρ listed in Table 2 and r_0 of 0.33.

TABLE 2: Plane Density (ρ) of Anthracene in a Single Layer

	$10^2\ \rho/nm^{-2}$	
sample	simulation[a]	experimental
A-0.5	0.78	2.2
A-1	1.2	4.7
A-3	1.8	10
A-4	3.0	14
A-6	8.8	25

[a] The values with which the best fitting results were achieved.

Results of the Simulation. The values used for the simulation are as follows. Förster radius R_0 was 2.5 nm and the unquenched lifetime τ_0 was 12.5 ns. Despite being determined in a solution, the value of R_0 is acceptable even for the LB film because the results of the simulation and the experiment agreed for the three-dimensional film, as described in the previous subsection. The layer separation d was 1.1 nm, as reported for a PiBMA LB film.[26] The appropriate value of L was harder to determine. Whereas a small simulation area reduces the load of the computer used, it restricts the diffusion length of excitons and may yield different results. We determined accordingly the appropriate size by testing for various simulation areas and found that 30−40 nm was adequate for L. The value of ρ is calculated from N and L.

Figure 9 shows the simulated decays compared with the experimental decays. As mentioned in the previous section, anomalous rises from the PVPe emission were found at short times for the small fraction samples; accordingly, the data points of the rises are not plotted for clarity. The best fits to the experimental curves were achieved by using the values of ρ listed in Table 2 and $r_0 = 0.33$.

Figure 10 shows the time evolution of the number of hopping h and mean-square displacement $\langle l^2\rangle$ obtained with the best fits of $r_{sim}(t)$. One can see that the number of hopping linearly increases with both time and the fraction. For A-4, as an example, the exciton hops ca. 100 times during the lifetime of the anthracene, 12.5 ns. Similarly, the mean-square displacement increases with both time and the fraction. However, the rises with time are not linear: the gradient gradually becomes gentler at short times. This means that the diffusion of the exciton does not follow Fick's law with a constant diffusion coefficient. This

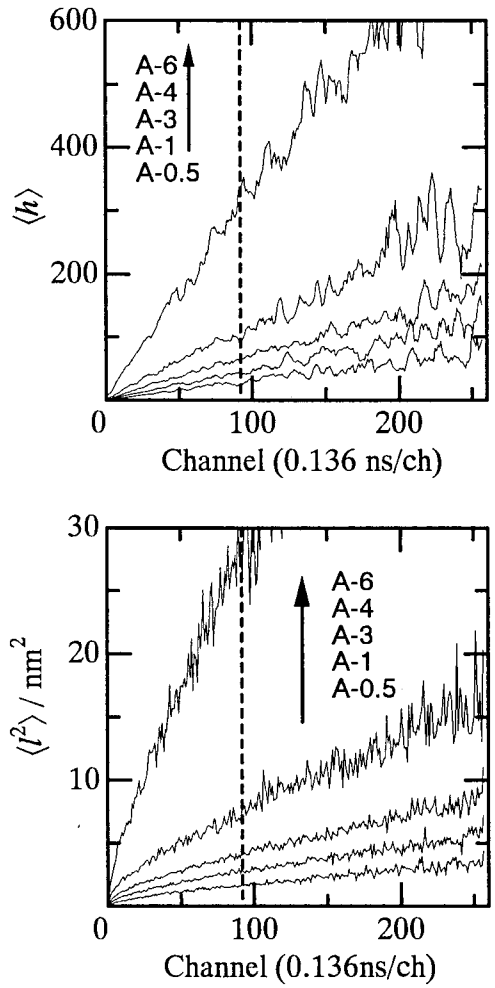

Figure 10. Time evolution of the number of exciton hopping $\langle h \rangle$ (*top*) and the square displacement $\langle l^2 \rangle$ from the origin (*bottom*), which are obtained from the best-fit simulation. The value of $\langle h \rangle$ increases with time and fraction. The value of $\langle l^2 \rangle$ also increased with time and the fraction, but the gradient with time becomes gradually gentler at short times. The dashed lines indicate the lifetime of anthracene, 12.5 ns.

behavior of diffusing excitons, which were also theoretically predicted by the Gochanour et al.,[24] is understood as follows. When the chromophores are randomly distributed and the density of them is low, there is a case that some chromophores form a small cluster. In this case, an exciton moves around the chromophores only within the cluster and is hard to travel farther out of the cluster. For A-4, $\langle l^2 \rangle$ is 7 nm^2 at 12.5 ns; that is, the exciton diffuses ca. 2.6 nm during the lifetime of anthracene, which is nearly equal to the Förster radius: $R_0 = 2.5$ nm.

As shown in Figure 9, the profiles of the experimental anisotropy decays are well described by this simulation. However, the values of ρ listed in Table 2 are different between the experiment and the simulation. To explain this discrepancy, we have to consider the orientation of the chromophores, because the Förster kinetics is strongly subject to the orientation of the transition moment vectors. For another possible manner of orientation, we considered a case that the moment vectors are positioned along the surface of a cone with a cone angle of 45° in the quasi-two-dimensional film. For the exact two-dimensional case, this cone model gives the orientation factor, κ^2, smaller than the random and isotropic orientation; that is, the value of ρ for the best-fit simulation becomes larger and approaches the experimental value. According to this model, we performed the simulation again, and as a result, the simulated curves reproduced the experimental decay. Nevertheless, contrary to our expectation, the values of ρ for the best fits become a little smaller (e.g., 0.025 nm^{-2} for A-4). The cause for this may be attributed to the fact that a double layer system is not exactly two-dimensional. Anyhow, these values are far smaller than the experimental ρ value, and thus, the preferential orientation is not the principal cause for the disagreement between the simulation and the experiment.

Next, since relaxation of the layer structure was also suspected of causing this disagreement, we carried out the computation taking account of the dispersion of the chromophores normal to the film plane. The ρ values became closer to the experimental values; however, the fit of simulated decay curves with the experimental ones got obviously worse.

Considering other possible reasons, we finally ascribed the observed slow migration rates to the statistical nonuniformity of the chromophore distribution. Judging from the fluorescence excitation spectra, we supposed the statistically uniform distribution of the anthracene chromophores in the two-dimensional plane. However, owing to the strong hydrophobic interaction among the aromatic rings, the chromophores tend to gather together. Although this nonuniformity was not detectable by spectroscopic observation, it might affect the process of energy migration. Surface pressure−area isotherms told us that the monolayers were stiffened at high contents of the chromophore, at which the monolayers formed excimers. These are experimental indications that the anthracene chromophores are likely to get close. The simulation at small chromophore fractions revealed that diffusion of excitons is retarded, owing to the stagnation in the small clusters of chromophores. Therefore, the present disagreement suggests the weak aggregation of the chromophores in the monolayer, resulting in the less efficient migration compared to that for a uniform distribution.

In any event, judging from the fact that profiles of the simulated curves conform to those of the experimental decays, it is safely said that the present simulation well describes the feature of quasi-two-dimensional migration of excitation energies which were characterized by the number of hopping, diffusion length, and their time evolution.

Conclusion

To clarify the nature of photophysical processes in a quasi-two-dimensional field, we investigated the fluorescence anisotropy of the anthracene-labeled poly(isobutyl methacrylate) layers included in LB films as adjacent two layers. The time-resolved fluorescence depolarization measurement revealed that the excitation energy migration between the anthracene moieties became more efficient as the anthracene fraction increased. As the anthracene fraction increased further, excimer-forming sites appeared and the excitation energy was trapped there via the efficient energy migration. A computer simulation based on the Monte Carlo method was applied to the anisotropy decays to elucidate the mode of the migration. The simulated anisotropy decay curves reproduced the profiles of the experimental decays, and the number of hopping and the square displacement of the migrating excitons were also obtained. An increase in anthracene fraction led to the increase in both the number of hopping and the mean-square displacement. For a given fraction, both are also increased with time, but the increment of the mean-square displacement gradually got smaller. This result arises from the property that the exciton tends to stay in small clusters of the chromophores, especially for the small plane density.

Acknowledgment. This work was supported by a Grant-in-Aid for Scientific Research (B) (No. 09450360) from the Ministry of Education, Science, Sports and Culture of Japan.

References and Notes

(1) Hayashi, T.; Okuyama, T.; Ito, S.; Yamamoto, M. *Macromolecules* **1994**, *27*, 2270.

(2) Yamamoto, M.; Kawano, K.; Okuyama, T.; Hayashi, T.; Ito, S. *Proc. Jpn. Acad.* **1994**, *70(B)*, 121.

(3) Hayashi, T.; Ito, S.; Onogi, Y.; Yamamoto, M.; Matsumoto, A. *Eur. Polym. J.* **1997**, *33*, 607.

(4) Hayashi, T.; Ito, S.; Yamamoto, M.; Tsujii, Y.; Matsumoto, M.; Miyamoto, T. *Langmuir* **1994**, *10*, 4142.

(5) Hayashi, T.; Mabuchi, M.; Mitsuishi, M.; Ito, S.; Yamamoto, M.; Knoll, W. *Macromolecules* **1995**, *28*, 2537.

(6) Ohmori, S.; Ito, S.; Yamamoto, M. *Macromolecules* **1991**, *24*, 2377.

(7) Ueno, T.; Ito, S.; Ohmori, S.; Onogi, Y.; Yamamoto, M. *Macromolecules* **1992**, *25*, 7150.

(8) Martin, T. J.; Webber, S. E. *Macromolecules* **1995**, *28*, 8845.

(9) Caldérara, F.; Hruska, Z.; Hurtrez, G.; Lerch, J.-P.; Nugay, T.; Riess, G. *Macromolecules* **1994**, *27*, 1210.

(10) Tcherkasskaya, O.; Spiro, G. J.; Ni, S.; Winnik, M. A. *J. Phys. Chem.* **1996**, *100*, 7114.

(11) Tcherkasskaya, O.; Ni, S.; Winnik, M. A. *Macromolecules* **1996**, *29*, 610.

(12) Ni, S.; Zhang, P.; Wang, Y.; Winnik, M. A. *Macromolecules* **1994**, *27*, 5742.

(13) Kuhn, H.; Möbius, D.; Bucher, H. In *Physical Methods of Chemistry*; Weissberger, A., Rossiter, B. W., Eds.; Wiley: New York, 1972; Vol 1, Part 3B, p 577.

(14) Yamazaki, I.; Tamai, N.; Yamazaki, T. *J. Phys. Chem.* **1990**, *94*, 516.

(15) Ichinose, N.; Nishimura, Y.; Yamazaki, I. *Chem. Phys. Lett.* **1992**, *197*, 364.

(16) Tamai, N.; Mutsuo, H.; Yamazaki, I. *J. Phys. Chem.* **1992**, *96*, 6550.

(17) Ito, S.; Ohkubo, H.; Ohmori, S.; Yamamoto, M. *Thin Solid Films* **1989**, *179*, 445.

(18) Ito, S.; Ohmori, S.; Yamamoto, M. *Macromolecules* **1992**, *25*, 185.

(19) Ohmori, S.; Ito, S.; Yamamoto, M. *Macromolecules* **1990**, *23*, 4047.

(20) Ohmori, S.; Ito, S.; Yamamoto, M. *Ber. Bunsen-Ges. Phys. Chem.* **1989**, *93*, 815.

(21) Gochanour, C. R.; Andersen, H. C.; Fayer, M. D. *J. Chem. Phys.* **1979**, *70*, 4254.

(22) Loring, R. F.; Andersen, H. C.; Fayer, M. D. *J. Chem. Phys.* **1982**, *76*, 2015.

(23) Loring, R. F.; Fayer, M. D. *Chem. Phys.* **1982**, *70*, 139.

(24) Gochanour, C. R.; Fayer, M. D. *J. Phys. Chem.* **1981**, *85*, 1989.

(25) Baumann, J.; Fayer, M. D. *J. Chem. Phys.* **1986**, *85*, 4087.

(26) Naito, K. *J. Colloid. Interface Sci.* **1989**, *131*, 218.

(27) Ulman, A. In *An Introduction to Ultrathin Organic Films From Langmuir−Blodgett to Self-Assembly*; Academic Press: San Diego, CA, 1991; p 123.

(28) Equation 1 holds on the assumption of the isotropic orientation of the transition moment vectors. In this work, we did not directly check this precondition. However, it is likely that the local relaxation of polymer segments after the deposition leads to the relaxation of some preferential orientation. As indirect evidence for this, the fluorescence decays obtained from eq 1 showed one-component exponential decays at small anthracene fractions when the influence of the PVPe emission was eliminated.